OPEN ACCESS PEER REVIEW

DOI: https://doi.org/10.52756/lbsopf.2024.e03.008

Chapter- 8

Pyrococcus abyssi's Methionine-tRNA Synthetase Exhibits Hyperthermophilic Signatures in Its Weak Forces and Cavities

Sahini Banerjee[1 #] and Amal Kumar Bandyopadhyay[2#*]

Keywords: Salt-bridge and microenvironment, energetics, weak forces, interior cavity

Abstract: Weak forces, including the salt-bridge and the inner cavity, are of particular importance in protein folding and functioning in extreme environments. A comparative study on these may reveal insights into the intrinsic protein thermostability. Here, we study salt-bridge energetics and its microenvironment, other weak interactions, and interior cavity properties of Methionine-tRNA synthetase from hyperthermophilic, *Pyrococcus abyssi* (PMRS) and mesophilic, *E. coli* (EMRS). Results show that PMRS, which is more hydrophilic, is uniquely distinct from EMRS. PMRS's complete and domain-specific sequences are favorable for more salt-bridges and other weak interactions than EMRS's. In the former, the recruitment of excess networked, long-ranged, and inter-domain salt bridges with energetically advantageous pairs and ME around them suggests that these properties originate from the underlying sequence. The fact that the net stability (ΔΔGnet) per salt bridge of PMRS exceeds that of EMRS denotes a novel design in its salt bridge. Furthermore, compared to EMRS, an excess of hydrogen bonds (HyB), hydrophobic, and other electrostatic interactions in PMRS's core and surface demonstrate that these also contribute to its thermostability. Notably, PMRS has a much lower level of water-mediated HyB than EMRS, pointing to an altered strategy. In addition, compared to EMRS, a lower and higher mostly empty interior cavities in PMRS's core and surface, respectively, indicate that surface engineering is more prominent in PMRS. We think that these differences are indeed related to the thermostability of the PMRS, which would apply to other similar systems.

Introduction:

The crystal structure of protein reveals the arrangements and interactions of the atoms, secondary structures, cavities, and shell-waters of the protein. A general insight into protein thermostability was found from a comparative study of mesophilic and thermophilic proteins (Vogt et al., 1997; Menéndez-Arias and Argosf, 1989; Szilágyi and Závodszky, 2000; Banerjee et al., 2021). Such knowledge helps to understand the basic mechanisms of protein function at high temperatures on the one hand and the practical applications on the other (Vogt et al., 1997). Although the topologies of orthologous proteins of normal and stress environments are similar, considerable differences exist in their homologous position in their sequence (Vogt et al., 1997;

Sahini Banerjee
Department of Biological Sciences, Indian Statistical Institute, Kolkata, West Bengal, India
E-mail: sahinib2@gmail.com **; Orcid iD:** https://orcid.org/0000-0002-0493-4797
***Amal Kumar Bandyopadhyay**
Department of Biotechnology, The University of Burdwan, Burdwan, West Bengal, India
E-mail: akbanerjee@biotech.buruniv.ac.in **; Orcid iD:** https://orcid.org/0000-0003-3499-5491
***Corresponding Author**: akbanerjee@biotech.buruniv.ac.in

Dr. Somnath Das, Dr. Jayanta Kumar Das, Dr. Mayur Doke, Dr. Vincent Avecilla (eds.), Life as Basic Science: An Overview and Prospects for the Future Volume: 3. ISBN: 978-81-978955-7-9;
pp. 180-208; Published online: 30th November, 2024

Menéndez-Arias and Argosf, 1989; Banerjee et al., 2021). The same topology is formed by the interplay of weak forces and secondary structures arising from the intrinsic sequence properties (Anfinsen, 1973; Dill, 1990). Protein-thermostability is due to various mechanisms such as an increase of ion-pair, HyB, polar surface, and helical structure, a decrease of flexible loops, and packing of amino acid residues (Vogt et al., 1997; Menéndez-Arias and Argosf, 1989; Hurley et al., 1992; Russell et al., 1997; Yip et al., 1998; Kumar et al., 2000; Banerjee et al., 2021; Sumida et al., 2024). In the case of thermophilic proteins, the number of low-volume cavities also increases (Vogt et al., 1997; Sternke et al., 2019; Biswas et al., 2020), whose importance in protein thermostability is not so clear (Vogt et al., 1997; Dubey and Jagannadham, 2008). Using the Poisson-Boltzmann Equation based method, it was demonstrated that compared to the mesophilic counterpart, the average electrostatic strength of thermophilic glutamate dehydrogenase and prolyl oligopeptidase increases as the number of salt bridges increases (Kumar et al., 2000; Banerjee et al., 2021). The net-stability of salt-bridge is derived from the sum of three-component terms, such as energetically costly desolvation-term ($\Delta\Delta G_{dslv}$), contributing bridge-term ($\Delta\Delta G_{brd}$), and background-term ($\Delta\Delta G_{bac}$) (Nayek et al., 2014; Nayek et al., 2015; Bandyopadhyay et al., 2019; Bandyopadhyay, 2020; Banerjee et al., 2021). The latter is formed by a handful of residues around the salt-bridge (i.e., the ME) that interact with the positive and negative partners of the salt-bridge (Bandyopadhyay, 2020; Banerjee et al., 2021). Although, in principle, it can be costly or contributing, it has been demonstrated that compared to the mesophiles, thermophile's ME plays a crucial role in protein thermostability (Banerjee et al., 2021; Banerjee et al., 2021). Although aromatic and bulky aliphatic residues' side-chain mediated interactions such as π-π, π-σ, π-amide, π-alkyl, alkyl\alkyl, are important in protein thermostability (Puchkaev et al., 2003; Martinez and Iverson, 2012), these are less studied. Similarly, like the above-mentioned salt bridges and HyBs, it is particularly interesting to understand the importance of other electrostatic interactions, such as π-cation, π-anion, π-HyB, etc., in thermostability (Mecozzi et al., 1996).

Methionine-tRNA ligase (EC:6.1.1.10) from *Pyrcoccus abyssi* (PMRS) and *E. coli* (EMRS) are cytosolic and class-I type enzymes that participate in elongation and initiation of protein synthesis (Crepin et al., 2003; Crepin et al., 2004). The enzyme, in structure, has five distinct domains such as Rossmann, Connective peptide (CP), KMSKS, anticodon, and C-terminal (Crepin et al., 2004). In this context, it is pertinent to understand hyperthermophilic features of PMRS by the use of only available crystal structure, 1RQG relative to its most high-resolution mesophilic counterpart i.e., 1PG2 from *E coli*.

Here, we have done a comparative study of PMRS and EMRS for the above-mentioned concerns. We apply various in silico methods to extract the sequence and structural properties of these proteins to understand their importance in the thermostability of PMRS in the background of EMRS. We believe that our work reveals heitherto unknown insights, which will find application in other similar systems.

Materials and methods:

Sequence and salt-bridge:

Complete and domain-specific sequences of PMRS (722 residues) and EMRS (677 residues) were analyzed using PHYSICO2 (Banerjee et al., 2015). The normalized relative composition of PMRS was plotted using Sigma Plot v12.0. Hoop-Woods hydrophilicity and Kyte-Doolittle hydrophobicity (Banerjee et al., 2015) were computed using an aligned sequence. The absolute frequency of SBFRs was determined from the sequence and salt-bridge (IP and NU) of PMRS and EMRS's structure. From these two, SBFR's normalized frequency used at the salt-bridge was determined. Six pairs, such as HD, HE, RD, RE, KD, and KE can take part in the salt-bridge. The frequencies of these pairs were compared for an equal length of 1RQG (606 residues) and 1PG2 (488 residues).

Salt-bridge energetics:

There are two types of salt-bridge, namely IP and NU. The binary properties of these salt-bridges (such as long-ranged vs. short-ranged, core vs. surface, etc.) were extracted using SBION2 (Gupta et al., 2015; Banerjee et al., 2021). Inter-domain salt-bridge was determined manually. IPM method was followed as earlier for the extraction of IP salt-bridge's energy terms using the PDB2PQR (Dolinsky et al., 2004) and APBS (Baker et al., 2001) programs (Nayek et al., 2014; Banerjee et al., 2021). The energy terms for NU salt-bridge were extracted using the NUM method, since, unlike IP, NU is made up of more than two salt-bridge partners (Bandyopadhyay et al., 2019; Banerjee et al., 2021). The net energy of a salt-bridge is the sum of the component energy terms. Average accessibility was determined using NACCESS program (Banerjee et al., 2021; Banerjee et al., 2021).

Microenvironment of salt-bridge:

Practically only a few residues of protein (~ 1-2%) contribute most of the background energy of a salt-bridge (Bandyopadhyay, 2014; Banerjee et al., 2021). These residues (mostly charged and polar types) orient around the positive and negative partners of the salt-bridge to interact with them. These residues are called ME-residues and their interaction energy is ME-energy (Bandyopadhyay, 2014; Banerjee et al., 2021). After obtaining the background energy by the above-mentioned method, a low energy cut-off is set on it to get the ME-residues and their energy. ME-residues' accessibility was computed using NACCESS program. ME-residues' secondary structure details are extracted from the PDB file itself. Other attributes are manually or programmatically configured if not mentioned otherwise (Bandyopadhyay, 2014; Banerjee et al., 2021).

Hydrogen bonds and other weak interactions:

Depending on the accessibility of the residue, the core and surface residues of the protein were separated and saved as different PDB files. Thus, during such a division of the residue, the shell waters that are within 3.9Å of the residues' atoms were also included in the PDB. It was used as

an input to BIOVIA Discovery Studio 2020 and HyBs, hydrophobic, and other electrostatic interactions were extracted using default parameters. The total number of interactions in the output file and their nature are huge, for example, the 1PG2_Core fraction has a total of 887 interactions (535 HyBs, 316 hydrophobic, and 36 electrostatic). In this inter-residue interaction, each type was normalized using the total Interactions. The same types of PMRS and EMRS subcategories were then compared.

Interior cavity:

The inner cavity of the protein was computed using the default parameters of the Surface_Racer program (Tsodikov et al., 2002). If shell-waters are within 3.9 Å of an atom of a cavity, those are included in the cavity. Surface_Racer determines the relative accessibility of the cavity atoms. The secondary structure details of the cavity atoms were taken from the PDB file. All this information is included together to create a PDB file. In this way, PDB files of all the cavities obtained from the protein were made. These PDB files were analyzed for shell-water content, secondary structure type, and residue class. The average and normalized values of each item were compared between PMRS and EMRS.

Results and discussion:

The sequence and the salt-bridge properties are interrelated:

The properties of the protein structure are derived from the underlying properties in its sequence (Anfinsen, 1973; Dill, 1990). The different forms of this property, therefore, seem to be the main source of deliberate living of hyperthermophiles in their extreme environments. Here, we see that hyperthermophilic, PMRS's sequence is much more hydrophilic than that of EMRS (Fig. 1a). The primary reason for this seems to be in the charged residues (Glu, Arg, Lys), as PMRS is relatively less in most polar residues (Ser, Thr, Asn, Gln) than in EMRS's (Fig. 1b) of which Asn, Gln are thermolabile (Russell et al., 1997).

(a) Hopp-Woods average hydrophilicity of PMRS (red) and EMRS (green). (b) Relative residue composition of PMRS. (c) Kyte-Doolittle hydrophilicity of PMRS (red) and EMRD (green). (d) SBFR's ratio in salt-bridge to the sequence. (e) PMRS and EMRS's salt-bridge pairs' frequency in 606 residue protein. (f) Details of a typical highly stable inter-domain networked unit in the core of PMRS. (g) Correlation between desolvation-term and ASAav for PMRS and EMRS. (h) Total desolvation-energy. (i) Total bridge-energy. (j) Correlation between bridge-term and ASAav for PMRS and EMRS. (k) Correlation between background-term and ASAav for PMRS and EMRS. (l) Total background-energy (m) Net-energy. (n) per salt-bridge stability. (o) Overall ME-energy.

In addition, the relative abundance of bulky hydrophobic residues (Ile, Val, Leu) in PMRS's sequence is noticeable in abundance. Although relative compositions of PMRS's domains (Fig. 2) are almost similar, some observations are very characteristic (Fig. 3a, b, c, d, e, f). The predominance of only acidic (Glu) and basic (Arg, Lys) residues in PMRS's KMSKS and CT (C-terminal) domains (Fig. 3c, e), respectively, may point towards the enhancement of inter-domain interaction specificity. The relative abundance of Cyseine that coordinates Zn^{++} (Crepin et al.,

2003) is only present in the CP domain (Fig. 2 and Fig. 3b) might be for its thermolabile nature (Russell et al., 1997). The decline in PMRS's higher level of hydrophobicity compared to EMRS's after the KMSKS domain (Fig. 1c) may indicate that the hydrophilicity of the charged residues of anticodon and CT domains supersedes the hydrophobic effect (Fig. 3d, e).

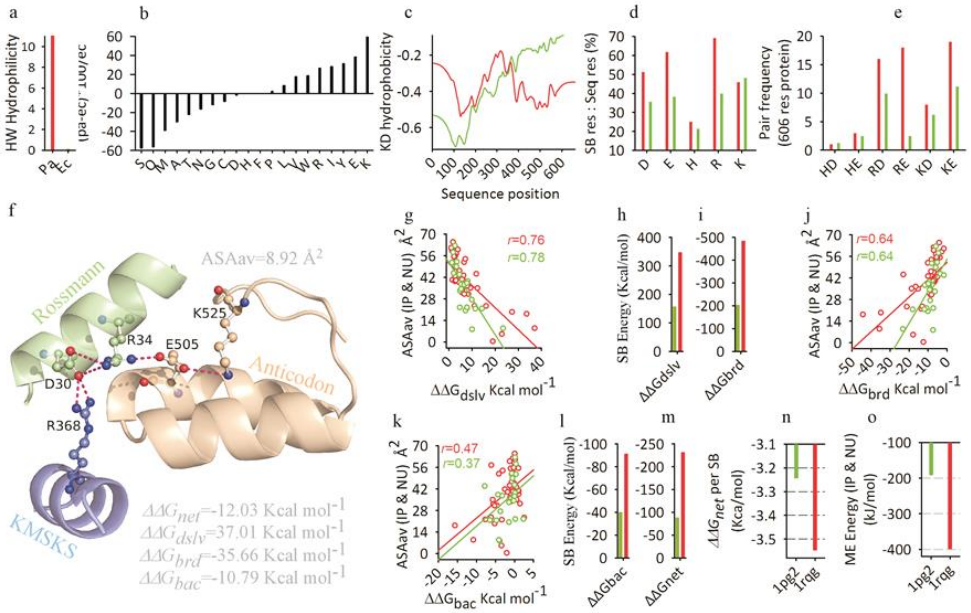

Figure 1: Sequence and salt-bridge properties of PMRD (Pa) and EMRS (Ec).

Figure 2: Crystal structure portion (488 for *E. coli* PDB, 1PG2 and 601 for *Pyrococcus abyssi* PDB, 1RQG) with different domains of Methionyl tRNA synthetase from bacteria (ec, *E. coli*) and *Pyrococcus abyssi* (ab).

Named domains are Rossmann domain (have *HIGH* region; sequence range: 15-25 for ec, and 10-21 for ab), CP domain (Zn binding region; in between Rossmann regions; here, 126-185 residues are absent in the crystal structure of ec), MNKS domain (for ATP binding; 333-337 for ec and 344-348 for ab), Anticodon (in between MNKS regions), and C terminal extreme region (CeX). The tRNA binding region at the C-terminal end is not shown (575-677 for ec and 622-722 for ab).

Table 1: Inter-domain salt-bridges for hyperthermophilic, *Pyrococcus abyssi* (structure: 1RQG). ASAav, average accessibility; ASA-ac, accessibility of acid partner; accessibility of base partner; Dist, distance.

ROSSMANN's partner	CP's partner	Dist (Å)	ASAav (Å^2)	ASA-ac (Å^2)	ASA-bs (Å^2)
E256	H100	3.8	0.4	0.6	0.2
D298	R161	3.3	57.4	57.1	75.8
E325	R198	3.2	52.1	44.8	59.4
ROSSMANN's partner	MNKS's partner				
D30	R368	2.7	10.6	0	21.2
R84	D360	2.9	40.6	39.3	42
K297	D380	3.7	35.9	27.5	44.2
ROSSMANN's partner	ANTICODON's partner				
D34	E505	3.5	15.1	16.3	13.9
K86	D510	2.7	51.5	39.7	63.3
MNKS's partner	ANTICODON's partner				
E377	K453	4.1*	20.5	11.3	29.7
E377	R451	4.8*	32.5	11.3	53.7
MNKS's partner	CT's partner				
E341	K575	3.2	22.2	1.8	42.7

32.5% and 26.8% residues of PMRS and EMRS are salt-bridge forming residue (SBFR) types, respectively, of which 17.7% and 10.3% are forming salt-bridge. In the case of 1RQG, this fraction for the Asp, Glu, and Arg is much higher than 1PG2 (Fig. 1d). Interestingly, of the six possible salt-bridge pairs (Asp-Arg, Asp-Lys, Asp-His, Glu-Arg, Glu-Lys, and Glu-His), the frequency of Asp-Arg, Glu-Arg, and Glu-Lys, which are known to be energetically advantageous (Meuzelaar et al., 2016) and helix promoter (Williams, et al., 1987), is much higher in 1RQG (Fig 1e).

(a) 1PG2's crystal structure and its salt-bridge. Here, the salt-bridges of the inter-domain (R, Rossman i.e., greenish; CP, connective peptide i.e., blueish; AC, anticodon; M, KMSKS i.e., cyan and CT, C-terminal, i.e., brownish) are visible. (b) 1RQG's crystal structure and its salt-bridge. Here, the salt-bridges of the inter-domain. (c) A typical, long-ranged IP-type salt-bridge

of 1RQG, which is absent in 1PG2. (d) Salt-bridge's intervening-distance specific frequency. Here, the frequency in salt-bridge for the range ≤10 is shown differently as it has much higher frequency. (e) Comparison of the frequencies of 1RQG (red) and 1PG2's (green) residue-classes. (CR, charged-class; PO, polar-class; HB, hydrophobic class).

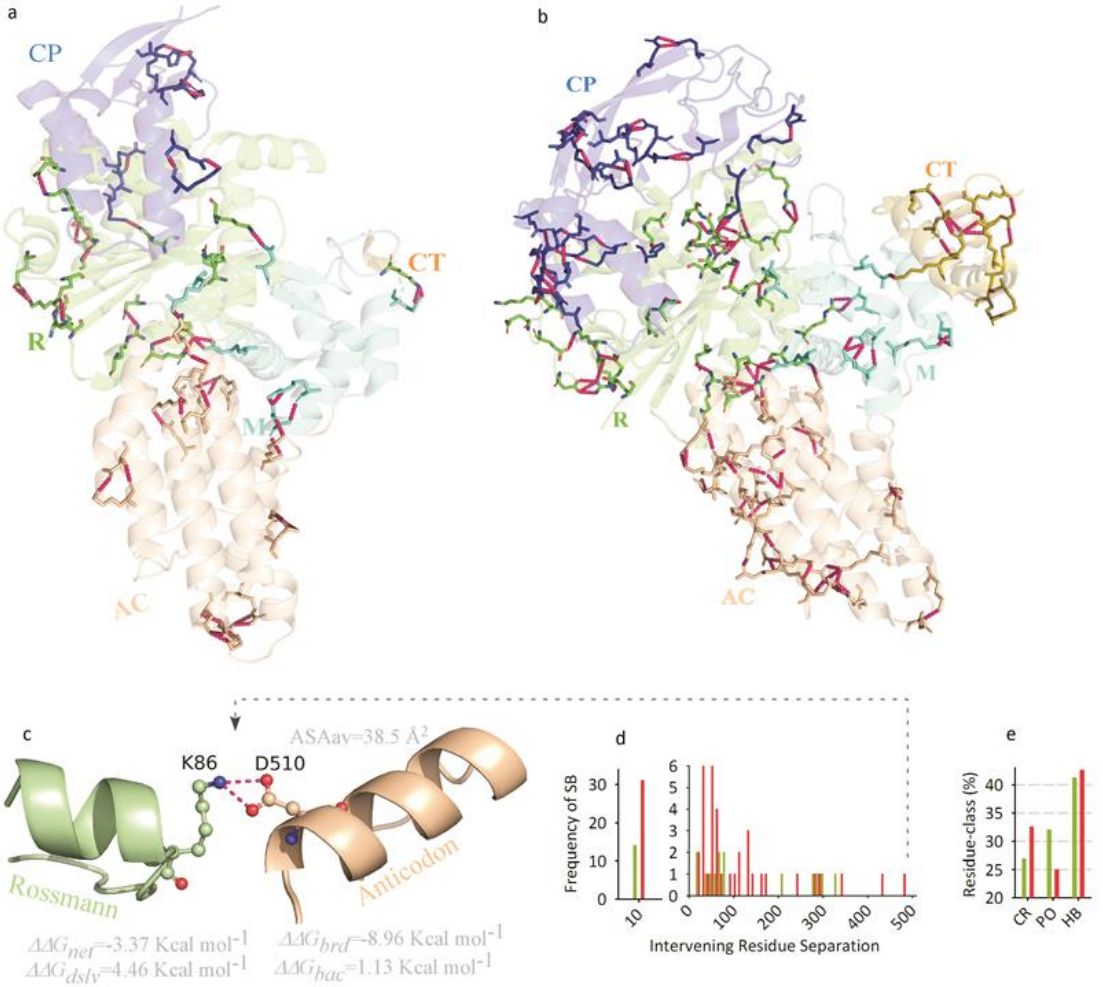

Figure 3: Unique features of salt-bridge in the structure of hyperthermophilic, *Pyrococcus abyssi* (structure: 1RQG) and mesophilic, *E. coli* (structure: 1PG2).

Notably, these have increased almost evenly in every domain as compared to 1PG2 (Fig. 4a-f). Again, the inter-domain salt-bridges are more exhaustive and high in frequency in 1RQG than 1PG2 (Table 1 and 2). Here, the question of whether the additional non-salt-bridge forming residues (nSBFRs) of the sequence (as isolated charged residue) are of any importance is relevant. The answer to this question may come from the energetics of salt-bridge (see below).

Relative composition of Rossmann (**a**), CP (**b**), MNKS (**c**), and anticodon (**d**) domains. pI of complete and domain-specific sequence of MetG tRNA synthetase (**e**). Comparison of normalized total charge (at physicological pH) of *E. coli* (circle) and *Pyrococcus abyssi* (triangle) for complete and region-specific sequences (f). Here, CeX is plotted separately for better visibility of other regions. Comparison of normalized net charge (at physicological pH) of *E. coli*

(circle) and *Pyrococcus abyssi* (triangle) for complete and region-specific sequences (g). Here, CeX is plotted separately for better visibility of other regions. Comparison of normalized GRAVY of *E. coli* (circle) and *Pyrococcus abyssi* (triangle) for complete and region-specific sequences (h). Here, CeX is plotted separately for better visibility of other regions.

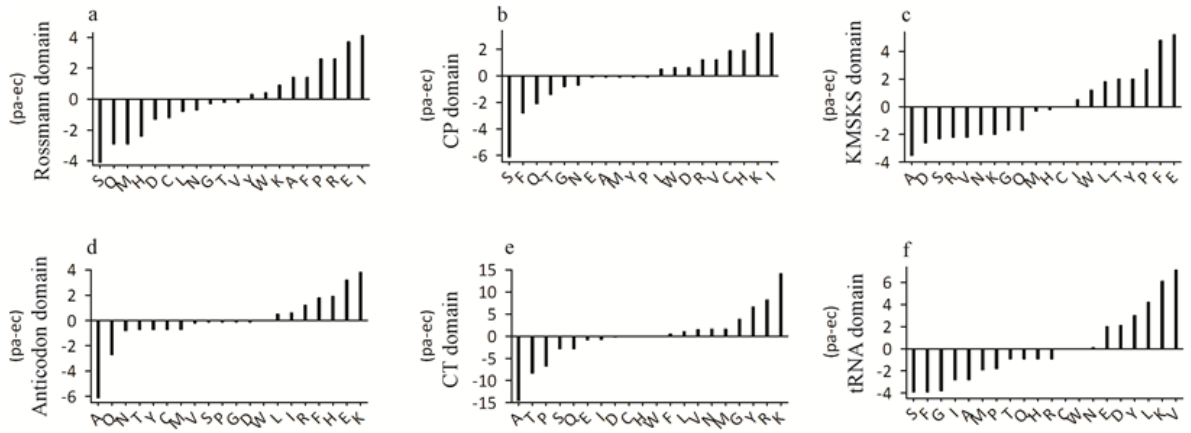

Figure 4: Relative (with reference to *E. coli*) composition and physicochemical properties of *Pyrococcus abyssi* MetG tRNA synthetase.

Table 2: Inter-domain salt-bridges for mesophilic, *E. coli* (structure: 1PG2). ASAav, average accessibility; ASA-ac, accessibility of acid partner; accessibility of base partner; Dist, distance.

ROSSMANN's partner	CP's partner	Dist (Å)	ASAav (Å^2)	ASA-ac (Å^2)	ASA-bs (Å^2)
H95	E101	2.7	22.4	21	23.9
ROSSMANN's partner	MNKS's partner				
D32	R356	2.7	7.2	0	14.3
K295	D369	3.1	37.5	31.1	44
MNKS's partner	ANTICODON's partner				
R366	E436	3.4	50.3	75	25.6
R384	K388	2.6	10.9	2.9	19

Per salt-bridge electrostatic strength is higher in PMRS:

In the former, on the one hand, as the long-ranged, inter-domain salt-bridge has increased (Fig. 4c and Fig. 1f), so has the number of complex networked, intra-domain, and core salt-bridge with more partners (Fig. 5a, b, Table 3-6).

(a) A typical intra-domain (Rossmann) and inter-helix complex networked core salt-bridge. As the salt-bridge is in the core, the desolvation cost is very high. At the same time the bridge energy term is also high. Further, the contribution of the microenvironment is also high. Sum of these three terms, i.e., $\Delta\Delta G_{net}$ is highest among all salt-bridges of the protein. (b) A typical intra-domain (Anticodon) and inter-helix complex networked core salt-bridge. Although, the

desolvation and bridge energy terms are similar as (a), the background term is weak. Here, the $\Delta\Delta G_{net}$ is moderately high, i.e., -12.9 Kcal/mol. This is a cyclic salt-bridge where all acidic and basic partners are interconnected to each-other.

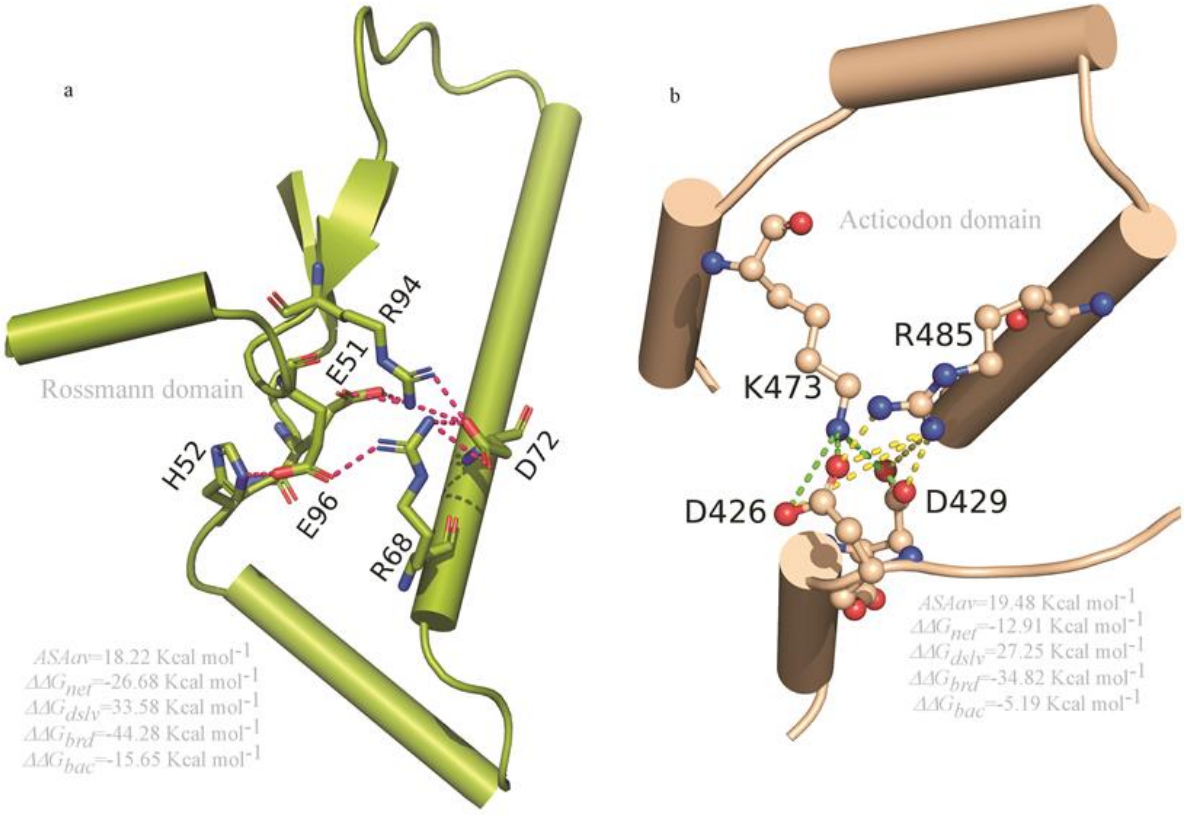

Figure 5: Intra-domain complex networked, core salt-bridge of hyperthermophilic, *Pyrococcus abyssi* (structure: 1RQG).

Table 3: Component and net energy terms, average-distance, and accessibility of isolated pair type of salt-bridge of 1PG2. Energy terms (in Kcal/mol) are extracted following the isolated pair method (IPM). The net energy of the salt-bridge is the sum of the component (desolvation i.e., $\Delta\Delta G_{dslv}$, bridge i.e., $\Delta\Delta G_{brd}$, and background i.e., $\Delta\Delta G_{bac}$) energy terms. Accessibility of acidic (A) and basic (B) residues was extracted by the ACCESS program, whose average is the ASA_{av}.

Salt-Bridge	$\Delta\Delta G_{dslv}$	$\Delta\Delta G_{brd}$	$\Delta\Delta G_{bac}$	$\Delta\Delta G_{net}$	AvDist	ASAav
LYS5_GLU288	4.8	-6.4	-1.5	-3.1	3.2	33.2
LYS316_GLU310	7.2	-10.1	-1.5	-4.3	3.2	20.4
LYS217_GLU220	1.9	-4.5	0.4	-2.3	3.3	58.2
LYS497_GLU500	2.1	-6.0	-0.8	-4.7	3.0	51.5
ARG469_ASP472	3.3	-6.0	-0.5	-3.3	2.7	48.9
LYS439_GLU443	2.1	-3.6	0.0	-1.5	3.1	44.7
HIS95_GLU101	4.8	-7.3	2.4	-0.2	2.7	22.4

LYS419_ASP423	2.7	-5.9	0.2	-3.1	3.2	62.5
ARG366_GLU436	4.6	-1.7	-7.8	-5.0	3.4	43.8
LYS295_ASP369	5.4	-8.0	-0.4	-2.9	3.1	37.5
LYS265_ASP269	5.3	-9.2	-0.2	-4.1	2.8	34.4
ARG103_GLU100	3.5	-5.2	-0.7	-2.4	3.7	52.1
HIS323_GLU27	10.0	-7.4	-3.8	-1.2	3.1	8.2
ARG403_ASP470	8.2	-9.5	0.1	-1.2	2.8	39.5
ARG395_ASP456	6.7	-9.4	-3.2	-5.9	2.9	37.6
LYS547_GLU544	1.4	-8.1	0.4	-6.3	2.8	51.5
ARG233_ASP230	6.7	-11.7	0.0	-5.0	3.0	37.2
LYS492_GLU503	7.9	-10.8	0.2	-2.8	2.6	22.4
ARG39_ASP92	9.9	-8.9	-3.7	-2.7	3.2	27.4

Table 4: Component and net energy terms of network unit type of salt-bridge of 1PG2 by network unit method (NUM). The net energy of the salt-bridge is the sum of the component (desolvation i.e., $\Delta\Delta G_{dslv}$, bridge i.e., $\Delta\Delta G_{brd}$, and background i.e., $\Delta\Delta G_{bac}$) energy terms. Accessibility of partners of NU residues was extracted by NACCESS program whose average is the ASA_{av}.

Salt-Bridge	$\Delta\Delta G_{dslv}$	$\Delta\Delta G_{brd}$	$\Delta\Delta G_{bac}$	$\Delta\Delta G_{net}$	AvDist	ASAav
R356-D32:R36-D32	23.4	-23.3	-4.1	-3.9	3.3	8.9
H189-D234:K248-D234	14.3	-12.0	-6.5	-4.1	2.9	21.7
K6-E44:K6-E279	7.8	-9.9	-4.3	-6.4	3.3	38.2
K388-D384:R380-D384	11.4	-18.1	-4.7	-11.4	2.9	21.6

Table 5: Component and net energy terms, average-distance, and accessibility of isolated pair type of salt-bridge of 1RQG. Energy terms (in Kcal/mol) are extracted following the isolated pair method (IPM). The net energy of the salt-bridge is the sum of the component (desolvation i.e., $\Delta\Delta G_{dslv}$, bridge i.e., $\Delta\Delta G_{brd}$, and background i.e., $\Delta\Delta G_{bac}$) energy terms. Accessibility of acidic (A) and basic (B) residues was extracted by the ACCESS program, whose average is the ASA_{av}.

Salt-Bridge	$\Delta\Delta G_{dslv}$	$\Delta\Delta G_{brd}$	$\Delta\Delta G_{bac}$	$\Delta\Delta G_{net}$	AvDist	ASAav
LYS575_GLU341	11.45	-11.12	-7.67	-7.34	3.21	22.2
LYS441_GLU445	2.73	-7.12	-0.45	-4.84	2.73	61.8
ARG231_ASP136	7.78	-13.61	-3.31	-9.14	3.02	21.9
ARG406_ASP471	6.34	-8.03	-0.87	-2.56	2.71	43.2
ARG3_ASP286	11.08	-13.06	-6.16	-8.14	2.82	23.5
LYS279_GLU321	5.67	-7.53	1.47	-0.39	2.61	32.4
ARG422_GLU531	4.42	-6.86	-2.54	-4.98	2.69	41.8
ARG198_GLU325	2.67	-5.48	-0.08	-2.89	2.87	52.1

ARG37_ASP90	8.47	-8.72	-4.58	-4.83	3.08	31.1
LYS477_GLU481	1.85	-4.17	0.09	-2.23	3.17	64.9
LYS280_GLU277	1.58	-6.25	-0.38	-5.05	3.21	40.3
ARG451_ASP454	2.86	-7.04	-0.03	-4.21	2.92	45.6
ARG183_GLU128	6.56	-10.1	-4.09	-7.63	3.13	51.8
LYS86_ASP510	4.46	-8.96	1.13	-3.37	2.7	38.7
LYS200_GLU221	5.76	-8.57	-0.75	-3.56	2.73	34
ARG84_ASP360	5.73	-7.09	1.14	-0.22	2.88	40.6
LYS79_GLU76	2.41	-7.06	0.01	-4.64	3.11	52.1
ARG391_ASP387	5.69	-9.24	-5.57	-9.12	2.9	32.1
ARG584_GLU588	3.89	-7.07	-1.24	-4.42	2.78	60
LYS389_ASP550	2.61	-6.72	0.26	-3.85	3.17	39.4
LYS152_ASP150	2.94	-6.79	1.02	-2.83	3.09	41
ARG161_ASP298	3.24	-5.88	-6.08	-8.72	2.96	57.4
HIS517_GLU513	2.25	-3.76	-1.01	-2.52	2.76	55.3
HIS100_GLU256	18.98	-12.45	-2.01	4.52	3.43	0.4
LYS120_GLU226	2.65	-5.11	0.14	-2.32	2.63	42.8
ARG430_GLU434	1.38	-2.84	-0.06	-1.52	2.63	59.1
ARG65_GLU73	4.6	-8.48	-0.8	-4.68	3	46.2
ARG526_GLU528	2.77	-4.97	-0.21	-2.41	2.68	55.8
ARG227_GLU225	2.23	-5.57	1.07	-2.27	2.76	55.5
LYS318_GLU323	1.01	-1.73	0.18	-0.54	3.73	61.1
LYS270_GLU267	3.08	-7.26	-1.79	-5.97	2.92	40

Table 6: Component and net energy terms of network unit type of salt-bridge of 1RQG by network unit method (NUM). The net energy of the salt-bridge is the sum of the component (desolvation i.e., $\Delta\Delta G_{dslv}$, bridge i.e., $\Delta\Delta G_{brd}$, and background i.e., $\Delta\Delta G_{bac}$) energy terms. Accessibility of partners of NU residues was extracted by NACCESS program whose average is the ASA_{av}.

Salt-Bridge	$\Delta\Delta G_{dslv}$	$\Delta\Delta G_{brd}$	$\Delta\Delta G_{bac}$	$\Delta\Delta G_{net}$	AvDist	ASAav
K249-D232:H187-D232:	22.9	-17.9	-3.4	1.6	3.1	5.2
R201-E197:R201-E204:	7.1	-8.2	-3.1	-4.2	2.9	53.9
K119-E243:K119-D245:	12.3	-15.3	-5.7	-8.7	3.2	35.0
K297-E336:K297-D380:	6.7	-8.2	-5.2	-6.8	3.1	31.1
R530-E523:K498-E523:	16.1	-21.2	2.6	-2.5	3.1	23.4
R599-E595:K587-E595:	4.5	-10.1	0.5	-5.0	2.6	43.2

R458-E435:K438-E435:R458-E442:	9.4	-18.7	0.6	-8.8	3.2	35.1
H52-E96:R94-E51:R94-D72:R68-D72:R68-E96:	33.6	-44.3	-15.7	-26.4	2.8	18.2
K110-E113:K110-E106:K102-E106:	8.0	-16.5	-1.1	-9.7	2.8	36.4
R368-D30:R34-D30:K525-E505:R34-E505:	37.0	-35.6	-10.8	-9.3	3.2	8.9
R570-E567:R570-D574:R579-D574:	11.9	-23.0	-1.2	-12.4	2.6	44.2
R485-D426:K473-D426:R485-D429:K473-D429:	27.3	-34.8	-5.2	-12.8	2.9	19.5

In some cases, these salt-bridges are of the self-neutralized (cyclic) (Fig. 5b) and secondary structures locking type (Fig. 4c, Fig. 1f and Fig. 5a, b). The abundance of such complexly designed salt-bridges in PMRS is largely unseen in EMRS. How does such a design of salt bridge affect its energetics? Several points are noteworthy in this aspect. First, PMRS has more core and intricate NU-type salt-bridges than EMRS (Table 4 vs. 6), and thus, the costly desolvation-term ($\Delta\Delta G_{dslv}$) is somewhat higher in PMRS (Fig. 1g, h). However, due to the recruitment of energetically advantageous and helix promoting pairs (Williams et al., 1987; Meuzelaar et al., 2016), the bridge-term ($\Delta\Delta G_{brd}$) has also been more contributing in PMRS than EMRS (Fig 1i, j) such that it causes an overall energy gain even after neutralizing the cost of $\Delta\Delta G_{dslv}$ (Table 3-6). These two terms, which rely solely on the salt-bridge partners (Bandyopadhyay et al., 2019; Bandyopadhyay, 2020; Banerjee et al., 2021), show an apparent linear relation to the protein's location-specific dielectric constant related parameter, ASAav (Fig. 1g, j). Second, unlike these two terms, the background term ($\Delta\Delta G_{bac}$) that relies on other residues of protein other than salt-bridge partners, and, which is equally likely to be costly or contributing, has been more contributing in PMRS and is almost unrelated to ASAav (Fig. 1k, l) indicating the involvement of other factors (Banerjee et al., 2021), which appears to be related with the intrinsic ME (Banerjee et al., 2021). Notably, the net ($\Delta\Delta G_{net}$) (Fig. 1m) and per salt-bridge (Fig. 1n) stability in PMRS is more favorable than that of the EMRS indicates a novel strategy. Third, since NU reduces desolvation cost more efficiently than IP (Bandyopadhyay et al., 2019; Banerjee et al., 2021), its higher level in PMRS seems to be a strategy (Table S4 vs. S6). ME, which is much more in PMRS due to an increase in sequence hydrophilicity than EMRS (Fig. 10), seems to be an intrinsic strategy. Overall, the change in the intrinsic property of the sequence seems to be the reason for the more favorable salt-bridges in PMRS.

Significance of ME in salt-bridge mediated thermostability:

ME-residues, which are mostly composed of charged and polar residue classes and derive from the underlying sequence, positioned themselves around the positive and negative partners

of salt-bridge and interacts with them (Banerjee et al., 2021). Here, several points are noteworthy. First, there are three ME-classes in charged-class. These are nSBME, IPME, and NUME (Table 7-10). Second, relative to EMRS, in PMRS, more nSBME act as ME-residues (Table 7 and Table 8), which explains why some of these do not participate in the salt-bridge, even though there is an excess of charged residues in the sequence. Third, due to the increase of salt-bridge, a higher proportion of ME-residues are also present in PMRS than EMRS. Along with the location at the core and surface of the salt-bridge, these MEs also orient themselves in those locations (Table 7-10). Fourth, the overall ME-energy is seen to be more contributing to PMRS than EMRS's, which appears to be largely due to energetically advantageous substitution at homologous positions in PMRS's sequence (Table 7-10). This is probably why its sequence hydrophilicity is much higher than that of its mesophilic counterpart (Nayek et al., 2015; Bandyopadhyay, 2020; Banerjee et al., 2021). Notably, although less polar class in PMRS than in EMRS, ME-energy is far greater in the former, which may indicate the proper use of selective polar residues. Surprisingly, the ME energy of the charged class has been less than the polar class might be for repulsive interactions between the salt-bridge partners and the charged ME residues. In the balance of protein rigidity and flexibility, this observation may have a beneficial role to play. Fourth, PMRS's ME-population is enriched in helix and also coil than EMRS's (Table 9). Finally, as ME-residue may interact with partners of more than one salt-bridge, the TU-value is greater than the actual counts of ME-residue (Table 7-10). This type of use seems to be particularly helpful in the structural integrity of the multi-domain protein. However, such exhaustive and overlapping usage of ME-residue is much more prominent in PMRS than EMRS and appears to play a crucial role in PMRS thermostability.

Table 7: Classes, categories, binary details, and interaction energies of microenvironment residues of 1RQG (606 residues). The energy cut-off=±0.75 kJ/mol. Co, core; su, surface; H, helix; S, strand; C, coil; TU, times used.

Res class	ME-class	nSBME	IPME	NUME	Total	co	su	Enz kJ/mol	H	S	C	TU
Charged	IP	20	6	14	40	11	29	-32.31	21	3	16	49
	NU	17	21	4	42	6	36	-10.59	16	5	21	49
	IP&NU	17	8	10	35	21	14	-55.07	18	4	13	92
Polar	IP	23	-	-	-	14	9	-129.73	17	4	2	23
	NU	17	-	-	-	12	5	-118.25	8	7	2	18
	IP&NU	6	-	-	-	3	3	-65.28	2	0	4	12
PG	IP	1	-	-	-	1	0	2.03	1	0	0	1

	NU	7	-	-	-	6	1	15.18	2	0	5	8
	IP&NU	2	-	-	-	2	0	-0.11	1	0	1	4
Hydrophobic	IP	0	-	-	-	0	0	0.00	0	0	0	0
	NU	3	-	-	-	3	0	-2.65	0	1	2	4
	IP&NU	1	-	-	-	1	0	-0.37	0	1	0	2
	Grand Total	**114**	**35**	**28**	**-**	**80**	**97**	**-397.14**	**86**	**25**	**66**	**262**

Table 8: Classes, categories, binary details, and interaction energies of microenvironment residues of 1PG2. The energy cut-off=±0.75 kJ/mol. H, helix; S, strand; C, coil; TU, times used.

	1pgm class of 1pg2 (488 Res)	nSBME	IPME	NUME	Total	co	su	Enz kj/mol	H	S	C	TU
CR	IP	13	7	4	24	5	19	-30.16	11	4	9	29
	NU	15	8	2	25	6	19	-9.37	19	5	1	26
	IP&NU	14	5	0	19	12	7	-48.75	10	2	7	44
PO	IP	20	-	-	-	13	7	-43.62	12	2	6	20
	NU	5	-	-	-	4	1	-35.90	2	3	0	5
	IP&NU	3	-	-	-	3	0	-30.18	0	1	2	6
PG	IP	3	-	-	-	3	0	-0.26	1	0	2	4
	NU	2	-	-	-	2	0	10.88	1	0	1	2
	IP&NU	0	-	-	-	0	0	0.00	0	0	0	0
	IP	1	-	-	-	1	0	-1.88	0	1	0	1
HB	NU	0	-	-	-	0	0	0.00	0	0	0	0
	IP&NU	1	-	-	-	1	0	-0.24	0	1	0	2
	Grand Total	**77**	**20**	**6**	**-**	**50**	**53**	**-189.48**	**56**	**19**	**28**	**139**

Table 9: Residue specific details of the microenvironment for isolated and network unit types of salt-bridge of 1PG2. Microenvironment (ME) residue can participate in isolated (IP) or network (NU) or both(IPNU) types of salt-bridge (SB). Thus, types of ME are of three types: IP_ME (ME for IP type of SB), NU_ME (ME for NU type of SB), and IPNU_ME ME for both IP and NU types of SB). Each residue (row-wise) is presented with residue name, residue ID as per the PDB file. ME_Energy is the interaction energy between the ME residue with the positive and negative partners of the concerned salt-bridge. An ME that can be either an IP partner (IP_ME) or an NU partner (NU_ME) or a non-salt-

bridge ME partner (nSBME) by itself can participate in the IP or NU or both types salt-bridge's microenvironment as a ME candidate. Residue-specific total interaction energy (ME_Energy) with the partners of salt-bridge is expressed in kJ/mol. Residue side-chain accessibility (ASA), type of secondary structure (Coil C, Helix H, and strand S) are also shown. Again, an ME residue can be used as an ME candidate for multiple salt-bridges. It has been denoted by the Times Used (TU) parameter. Only those residues were considered as ME-residue whose interaction energy was either greater than 0.75 kJ/mol (unstable) or less than -0.75 kJ/mol (stable). If a residue is ME for multiple times, the sum of the energy was not used as screening criteria.

Type of ME	Residue name	Residue ID	ME-Energy (kJ/mol)	ASA Å^2	SECONDARY STRUCTURE	Times Used	Type of partner SB (IP or NU) nSB
NU_ME	ARG	122	1.3228	55.9	S	1	nSBME
NU_ME	ARG	41	0.7853	42.4	H	1	nSBME
NU_ME	ARG	453	0.9133	66.7	H	1	nSBME
NU_ME	ARG	485	1.0376	6.2	H	1	nSBME
NU_ME	ARG	501	2.2538	44.8	H	1	nSBME
NU_ME	ASN	121	-0.9986	44.1	S	1	nSBME
NU_ME	ASP	278	0.7864	76.2	H	1	nSBME
NU_ME	ASP	351	-6.4147	34.9	H	1	nSBME
NU_ME	ASP	376	-3.6467	52.7	H	1	nSBME
NU_ME	ASP	449	-7.5481	49.5	H	1	nSBME
NU_ME	ASP	83	-1.2096	7	H	1	nSBME
NU_ME	GLU	188	-4.5967	55.9	S	1	nSBME
NU_ME	HIS	21	0.9332	26.5	H	1	nSBME
NU_ME	LYS	114	0.9407	56.7	H	1	nSBME
NU_ME	LYS	282	-2.2694	58.6	H	1	nSBME
NU_ME	LYS	362	2.5006	38.5	H	2	nSBME
NU_ME	PRO	493	2.136	0	C	1	nSBME
NU_ME	PRO	496	8.7403	3.9	H	1	nSBME
NU_ME	SER	187	-18.3885	19.5	S	1	nSBME
NU_ME	SER	232	-4.7789	0.1	S	1	nSBME
NU_ME	TYR	280	1.7722	0.6	H	1	nSBME
NU_ME	TYR	357	-13.51	0.1	H	1	nSBME
NU_ME	ARG	233	8.3635	36.1	S	1	IP
NU_ME	ARG	380	1.1995	42.8	H	1	NU
NU_ME	ARG	395	0.8532	21.5	H	1	IP
NU_ME	ASP	230	-8.6499	38.2	S	1	IP
NU_ME	ASP	384	-1.8952	2.9	H	1	NU
NU_ME	ASP	456	-0.8221	53.8	H	1	IP
NU_ME	ASP	92	2.5489	21.3	C	1	IP

NU_ME	GLU	27	-0.8644	9.3	H	1	IP
NU_ME	GLU	288	1.3147	27.1	S	1	IP
NU_ME	LYS	497	2.791	44.5	H	1	IP
IP_ME	ASN	102	-1.5138	0.4	H	1	nSBME
IP_ME	ASN	266	3.5294	20.5	H	1	nSBME
IP_ME	ASN	391	-1.4173	45.6	H	1	nSBME
IP_ME	ASN	396	-2.8365	0	H	1	nSBME
IP_ME	ASN	452	-12.1257	15.9	H	1	nSBME
IP_ME	ASN	93	-0.8118	14.1	S	1	nSBME
IP_ME	ASP	296	1.005	61.9	C	1	nSBME
IP_ME	ASP	368	-1.3897	64.8	C	1	nSBME
IP_ME	ASP	51	-1.9834	1.3	S	2	nSBME
IP_ME	CYS	11	-1.881	0	S	1	nSBME
IP_ME	GLN	104	-1.1144	65.8	H	1	nSBME
IP_ME	GLN	213	-1.2185	49.2	H	1	nSBME
IP_ME	GLN	30	2.5311	5.7	H	1	nSBME
IP_ME	GLN	466	-3.2526	49.1	C	1	nSBME
IP_ME	GLU	107	-4.8439	44.9	H	1	nSBME
IP_ME	GLU	212	-1.2791	78.1	H	1	nSBME
IP_ME	GLU	241	-2.5921	61.4	C	1	nSBME
IP_ME	GLU	411	0.9272	81.5	C	1	nSBME
IP_ME	GLU	433	-2.2742	40.1	C	1	nSBME
IP_ME	GLY	262	0.8528	0	H	1	nSBME
IP_ME	GLY	324	0.2795	0	C	2	nSBME
IP_ME	HIS	301	-4.3184	4	H	1	nSBME
IP_ME	HIS	80	-1.8035	0.6	H	1	nSBME
IP_ME	HIS	98	1.9319	35.6	C	1	nSBME
IP_ME	LYS	270	-0.5939	52	H	3	nSBME
IP_ME	LYS	283	-7.6117	46.3	C	1	nSBME
IP_ME	PRO	14	-1.3966	3.1	C	1	nSBME
IP_ME	SER	263	-1.5621	0.1	H	1	nSBME
IP_ME	SER	318	0.8864	22.5	C	1	nSBME
IP_ME	SER	364	-3.5692	31.9	C	1	nSBME
IP_ME	SER	365	-20.0916	12.4	C	1	nSBME
IP_ME	SER	394	0.8162	45.1	H	1	nSBME
IP_ME	SER	99	3.8422	8.9	H	1	nSBME
IP_ME	TYR	237	-0.8812	7.5	C	1	nSBME
IP_ME	TYR	260	-1.0041	1.1	H	1	nSBME
IP_ME	TYR	290	-2.7545	16.9	S	1	nSBME
IP_ME	TYR	325	-1.0673	59.1	C	1	nSBME
IP_ME	ARG	36	3.9893	26.6	H	3	NU

IP_ME	ASP	234	-0.9192	42.1	S	1	NU
IP_ME	ASP	269	2.3121	36.4	H	1	IP
IP_ME	ASP	32	-8.0664	0	H	1	NU
IP_ME	ASP	369	-2.9	44	C	1	IP
IP_ME	GLU	100	0.7595	72	H	1	IP
IP_ME	GLU	436	-0.7644	25.6	H	1	IP
IP_ME	GLU	44	1.0752	35.4	S	1	NU
IP_ME	HIS	95	-0.8721	21	S	1	IP
IP_ME	LYS	265	-2.6437	32.4	H	1	IP
IP_ME	LYS	295	2.6967	31.1	C	1	IP
IPNU_ME	ARG	271	-12.116	39	H	2	nSBME
IPNU_ME	ARG	315	-3.7326	8.8	C	3	nSBME
IPNU_ME	ARG	435	3.9613	10.7	C	3	nSBME
IPNU_ME	ARG	442	0.646	73.7	H	2	nSBME
IPNU_ME	ASN	46	-7.1105	0.1	S	2	nSBME
IPNU_ME	ASN	88	3.3187	18.9	C	2	nSBME
IPNU_ME	ASP	255	-6.3145	0.5	H	3	nSBME
IPNU_ME	ASP	273	5.245	15.3	C	2	nSBME
IPNU_ME	ASP	353	-21.7569	1.3	H	2	nSBME
IPNU_ME	ASP	52	2.3307	3.3	C	2	nSBME
IPNU_ME	GLU	509	-2.1962	75.6	C	2	nSBME
IPNU_ME	HIS	24	-2.1175	39.2	H	2	nSBME
IPNU_ME	HIS	28	-9.1918	1.8	H	2	nSBME
IPNU_ME	HIS	291	-5.1287	0	S	3	nSBME
IPNU_ME	HIS	43	0.1077	14.3	C	2	nSBME
IPNU_ME	HIS	54	5.1465	0.2	C	3	nSBME
IPNU_ME	PHE	47	-0.2388	0	S	2	nSBME
IPNU_ME	SER	90	-26.3875	16.4	C	2	nSBME
IPNU_ME	ARG	39	-2.7158	33.4	H	3	IP
IPNU_ME	GLU	500	-2.6301	58.5	H	2	IP
IPNU_ME	GLU	503	-1.6814	20.9	H	2	IP
IPNU_ME	HIS	323	0.1196	7	S	2	IP
IPNU_ME	LYS	492	3.2775	24	H	2	IP

Table 10: Residue specific details of the microenvironment for isolated and network unit types of salt-bridge of 1RQG. Microenvironment (ME) residue can participate in isolated (IP) or network (NU) or both (IPNU) types of salt-bridge (SB). Thus, types of ME are of three types: IP_ME (ME for IP type of SB), NU_ME (ME for NU type of SB), and IPNU_ME ME for both IP and NU types of SB). Each residue (row-wise) is presented with residue name, residue ID as per the PDB file. ME_Energy is the interaction energy between the ME residue with the positive and negative partners of the concerned salt-bridge. An ME that can be either an IP partner (IP_ME) or an NU partner (NU_ME) or a non-salt -bridge ME partner (nSBME) by itself can participate in the IP or NU or both types salt-bridge's microenvironment as a ME candidate. Residue-specific total interaction energy (ME_Energy) with the partners of salt-bridge is expressed in kJ/mol. Residue side-chain accessibility (ASA), type of secondary structure (Coil C, Helix H, and strand S) are also shown. Again, an ME residue can be used as an ME candidate for multiple salt-bridges. It has been denoted by the Times Used (TU) parameter. Only those residues were considered as ME-residue whose interaction energy was either greater than 0.75 kJ/mol (unstable) or less than -0.75 kJ/mol (stable). If a residue is ME for multiple times, the sum of the energy was not used as screening criteria.

Type of ME	Residue name	Residue ID	ME-Energy (kJ/mol)	ASA Å^2	SECONDARY STRUCTURE TYPE	Times Used	Type of partner SB (IP or NU) nSB (non SB)
NU_ME	ALA	186	-1.0743	14.1	S	1	nSBME
NU_ME	ARG	379	-2.108	78.3	C	1	nSBME
NU_ME	ASN	114	-1.1267	26.9	H	1	nSBME
NU_ME	ASN	335	-1.1178	8.7	S	1	nSBME
NU_ME	ASP	242	1.036	102.8	C	1	nSBME
NU_ME	ASP	331	1.2415	22.4	C	1	nSBME
NU_ME	ASP	482	-3.0462	44	H	1	nSBME
NU_ME	GLN	124	-9.1322	37.5	S	1	nSBME
NU_ME	GLU	166	-2.1892	77.2	C	1	nSBME
NU_ME	GLU	244	1.7658	83.3	C	1	nSBME
NU_ME	GLU	427	1.5903	98.1	H	1	nSBME
NU_ME	GLU	431	1.0963	57.2	H	1	nSBME
NU_ME	GLY	501	4.1481	0	H	2	nSBME
NU_ME	HIS	116	0.1216	21.7	C	2	nSBME
NU_ME	HIS	293	-1.0113	0.5	S	1	nSBME
NU_ME	HIS	472	1.1845	46.2	H	1	nSBME
NU_ME	HIS	536	8.3675	20	C	2	nSBME
NU_ME	LYS	191	0.9639	32.4	C	1	nSBME
NU_ME	LYS	209	-5.5604	53.5	H	1	nSBME
NU_ME	LYS	247	-0.347	62.2	C	2	nSBME
NU_ME	LYS	344	-0.9828	88.2	S	1	nSBME
NU_ME	LYS	606	2.0919	108.3	C	1	nSBME

NU_ME	MET	246	-2.5007	0.1	C	2	nSBME
NU_ME	PHE	133	0.9274	18.8	C	1	nSBME
NU_ME	PRO	240	0.9272	5.2	C	1	nSBME
NU_ME	PRO	28	1.1074	0	C	1	nSBME
NU_ME	PRO	376	-1.6134	1	C	1	nSBME
NU_ME	PRO	506	2.1667	0	C	1	nSBME
NU_ME	PRO	509	6.5422	8.1	H	1	nSBME
NU_ME	PRO	533	1.9015	55.2	C	1	nSBME
NU_ME	SER	185	-17.9638	9.5	S	1	nSBME
NU_ME	SER	461	2.1193	46.2	H	1	nSBME
NU_ME	SER	512	-30.7314	0	H	1	nSBME
NU_ME	THR	122	1.2366	29	S	1	nSBME
NU_ME	THR	230	4.3965	0	S	1	nSBME
NU_ME	THR	489	-1.2946	2.6	H	1	nSBME
NU_ME	THR	49	-13.8669	0	S	1	nSBME
NU_ME	TRP	235	-2.8618	16.9	C	1	nSBME
NU_ME	TRP	516	-5.0178	6.4	H	2	nSBME
NU_ME	TYR	112	-1.2563	50	H	1	nSBME
NU_ME	TYR	188	-17.2889	4.7	S	1	nSBME
NU_ME	TYR	314	-2.4072	5.9	C	1	nSBME
NU_ME	TYR	469	-19.1123	0.3	H	1	nSBME
NU_ME	TYR	602	-2.8232	4.5	H	1	nSBME
NU_ME	ARG	65	-0.8191	39.1	C	1	IP
NU_ME	GLU	73	0.7663	53.4	H	1	IP
NU_ME	ARG	84	1.2178	39.3	H	1	IP
NU_ME	LYS	86	4.5995	37.4	H	1	IP
NU_ME	ASP	90	0.9376	27.7	C	1	IP
NU_ME	LYS	119	5.3804	30.1	S	1	NU
NU_ME	LYS	120	2.8316	41.2	S	1	IP
NU_ME	ARG	161	-0.7991	68.7	C	1	IP
NU_ME	LYS	200	-13.8854	10	H	1	IP
NU_ME	GLU	221	8.9047	57.9	H	1	IP
NU_ME	GLU	225	-1.1613	68.9	C	1	IP
NU_ME	GLU	226	-1.2253	44.3	C	1	IP
NU_ME	ARG	227	1.9857	42.1	S	1	IP
NU_ME	GLU	243	-3.7	31.6	C	1	NU
NU_ME	ASP	245	-4.9659	43.2	C	1	NU
NU_ME	ARG	391	0.8623	34.5	H	1	IP
NU_ME	ARG	422	-0.1494	24.7	C	2	IP
NU_ME	ARG	430	-0.935	70	H	1	IP

NU_ME	ARG	458	1.2504	19.4	H	1	NU
NU_ME	ASP	510	-6.0814	40	H	1	IP
NU_ME	GLU	513	-11.1232	57.4	H	2	IP
NU_ME	HIS	517	3.476	53.2	H	1	IP
NU_ME	ARG	526	2.8417	52.1	C	2	IP
NU_ME	GLU	528	-2.8484	59.5	C	2	IP
NU_ME	GLU	531	-2.1616	58.9	C	1	IP
IP_ME	ARG	137	1.908	27.1	H	2	nSBME
IP_ME	ARG	271	-3.2062	63.7	H	1	nSBME
IP_ME	ARG	59	1.7813	41.4	H	2	nSBME
IP_ME	ASN	276	8.1087	61.8	C	1	nSBME
IP_ME	ASN	399	-0.796	26.8	H	1	nSBME
IP_ME	ASN	402	5.636	47.6	H	1	nSBME
IP_ME	ASN	467	-13.0092	14.4	H	1	nSBME
IP_ME	ASN	491	-14.057	2.8	H	1	nSBME
IP_ME	ASP	130	0.8901	21.7	C	1	nSBME
IP_ME	ASP	319	-1.0115	81	C	1	nSBME
IP_ME	ASP	42	-10.1651	47.6	S	2	nSBME
IP_ME	ASP	551	0.7996	56.6	H	2	nSBME
IP_ME	ASP	581	-2.033	47	H	2	nSBME
IP_ME	GLN	288	-9.698	38.4	C	1	nSBME
IP_ME	GLN	77	-1.3277	37.7	H	1	nSBME
IP_ME	GLU	149	0.8351	95.3	C	1	nSBME
IP_ME	GLU	157	-2.7898	51.1	C	1	nSBME
IP_ME	GLU	320	-2.5453	78.7	C	1	nSBME
IP_ME	GLU	357	0.8039	28.8	H	1	nSBME
IP_ME	GLU	41	0.7703	13.2	C	1	nSBME
IP_ME	GLU	63	-1.4641	47.5	H	1	nSBME
IP_ME	GLU	69	-2.5449	62.4	H	1	nSBME
IP_ME	GLY	260	2.0305	0	H	1	nSBME
IP_ME	HIS	268	-6.0303	8.1	H	2	nSBME
IP_ME	HIS	405	1.8099	55.1	H	1	nSBME
IP_ME	LYS	316	1.0981	72.4	C	1	nSBME
IP_ME	LYS	39	-2.5337	45.4	C	2	nSBME
IP_ME	LYS	457	-0.8622	77.3	H	2	nSBME
IP_ME	SER	104	-5.9616	0	H	1	nSBME
IP_ME	SER	181	-12.9052	27.3	S	1	nSBME
IP_ME	SER	263	-1.7311	0.3	H	1	nSBME
IP_ME	SER	384	-17.2879	23.5	H	1	nSBME
IP_ME	THR	289	-11.9535	1.7	S	1	nSBME
IP_ME	THR	54	-16.053	1.5	H	1	nSBME

IP_ME	THR	81	-1.8627	1.2	H	1	nSBME
IP_ME	TRP	278	-1.0982	11.3	H	1	nSBME
IP_ME	TYR	126	-2.536	18.8	S	1	nSBME
IP_ME	TYR	189	-1.6057	14.9	S	1	nSBME
IP_ME	TYR	252	-0.8824	29.3	H	1	nSBME
IP_ME	TYR	281	-1.0112	8.2	H	1	nSBME
IP_ME	TYR	370	-15.6696	0.5	H	1	nSBME
IP_ME	TYR	560	1.9456	20.8	H	1	nSBME
IP_ME	TYR	576	-14.8017	23.6	H	1	nSBME
IP_ME	TYR	577	-1.1728	12.8	H	1	nSBME
IP_ME	ARG	3	2.8145	15.8	S	1	IP
IP_ME	ASP	30	-8.2999	0	C	1	NU
IP_ME	ARG	34	2.3936	16.3	C	2	NU
IP_ME	GLU	51	-2.5145	0	C	1	NU
IP_ME	ASP	72	0.8184	41.3	H	1	NU
IP_ME	ARG	94	1.423	13.2	S	1	NU
IP_ME	LYS	102	1.0106	60.6	H	1	NU
IP_ME	GLU	197	-1.8345	61.8	H	1	NU
IP_ME	ARG	201	4.6109	61	H	1	NU
IP_ME	GLU	204	-7.7596	38.9	H	1	NU
IP_ME	GLU	277	0.8048	43.3	C	1	IP
IP_ME	LYS	280	2.5558	37.4	H	1	IP
IP_ME	ASP	286	-0.8984	31.1	C	1	IP
IP_ME	LYS	297	-2.6693	27.5	C	1	NU
IP_ME	GLU	321	1.1885	53.3	C	1	IP
IP_ME	GLU	336	1.3549	21.6	C	1	NU
IP_ME	ARG	368	-1.5757	1	H	1	NU
IP_ME	LYS	389	-0.8271	30.7	H	1	IP
IP_ME	GLU	435	0.8136	19.9	H	1	NU
IP_ME	LYS	438	-1.2326	56.1	H	1	NU
IPNU_ME	ARG	349	-1.9963	34.9	C	2	nSBME
IPNU_ME	ARG	539	3.6259	57	C	2	nSBME
IPNU_ME	ASP	154	-0.3218	72.1	C	3	nSBME
IPNU_ME	ASP	184	-2.4382	79.2	S	2	nSBME
IPNU_ME	ASP	365	-5.4679	5.9	H	2	nSBME
IPNU_ME	ASP	382	6.2772	41	S	3	nSBME
IPNU_ME	ASP	50	0.1984	15.8	C	3	nSBME
IPNU_ME	GLN	495	0.6853	0.2	H	2	nSBME
IPNU_ME	GLU	377	2.8516	10.1	C	3	nSBME
IPNU_ME	GLU	395	-11.795	37.4	H	2	nSBME

IPNU_ME	GLY	236	0.2928	0	C	2	nSBME
IPNU_ME	GLY	53	-0.3979	0	H	2	nSBME
IPNU_ME	HIS	18	-1.2938	19.4	H	3	nSBME
IPNU_ME	HIS	21	-1.4011	48.3	H	3	nSBME
IPNU_ME	HIS	303	-2.3218	3.2	H	2	nSBME
IPNU_ME	HIS	356	3.7468	21.8	H	2	nSBME
IPNU_ME	HIS	75	-13.6707	17.1	H	4	nSBME
IPNU_ME	LYS	213	-4.4662	26.3	H	2	nSBME
IPNU_ME	LYS	453	-2.2062	29.7	H	3	nSBME
IPNU_ME	LYS	514	1.4098	39.8	H	2	nSBME
IPNU_ME	PHE	45	-0.3661	0	S	2	nSBME
IPNU_ME	SER	88	-25.7323	17.5	C	2	nSBME
IPNU_ME	THR	95	-3.7044	0	C	2	nSBME
IPNU_ME	TYR	101	-15.1646	35.3	H	2	nSBME
IPNU_ME	TYR	12	0.2771	29.9	C	2	nSBME
IPNU_ME	TYR	337	-21.6394	47.4	C	2	nSBME
IPNU_ME	ARG	37	-4.7152	34.6	C	2	IP
IPNU_ME	HIS	52	-9.598	0.2	C	2	NU
IPNU_ME	HIS	100	18.8738	0.2	H	4	IP
IPNU_ME	ASP	136	-5.6937	25	H	3	IP
IPNU_ME	HIS	187	6.6996	0.4	S	5	NU
IPNU_ME	ARG	231	8.0118	18.7	S	4	IP
IPNU_ME	ASP	232	-2.268	10.7	C	2	NU
IPNU_ME	LYS	249	-1.4446	4.4	C	3	NU
IPNU_ME	GLU	256	-34.4997	0.6	H	3	IP
IPNU_ME	LYS	279	0.0894	11.5	H	2	IP
IPNU_ME	GLU	341	2.2417	1.8	C	2	IP
IPNU_ME	ASP	387	0.6113	29.7	H	2	IP
IPNU_ME	ASP	429	-5.1754	0	H	2	NU
IPNU_ME	LYS	498	8.0995	0.8	H	2	NU
IPNU_ME	GLU	505	0.8737	13.9	H	4	NU
IPNU_ME	GLU	523	-6.9789	22	C	2	NU
IPNU_ME	LYS	525	-4.4687	13.4	C	3	NU
IPNU_ME	ARG	530	3.5406	47.3	C	2	NU

Importance of non-salt-bridge weak interactions in thermostability:

(a) Comparison of inter-residue HyBs in core (co). (b) Comparison of inter-residue HyBs in surface (su). (d) A typical presentation of HOH-HOH and HOH-residue types of HyBs. (e) A typical presentation of different types of hydrophobic interactions. (g) Comparison of inter-residue hydrophobic interactions in the core. (h) Comparison of inter-residue hydrophobic

interactions in the surface. (i) Comparison of inter-residue electrostatic interactions in the core. (j) Comparison of inter-residue hydrogen bonds in the surface

To understand the role of hydrogen bonds, hydrophobic and other electrostatic interactions (Mecozzi et al., 1996; Puchkaev et al., 2003; Martinez and Iverson, 2012), their normalized frequency of the core and surface of the PMRS and EMRS have been compared. The frequency of HyBs at PMRS's core and the surface is much higher than that of EMRS (Fig. 6a, b, Table 11). Oppositely, the shell-water mediated HyBs dominate in EMRS (Fig. 6c, d, e). Aromatic π-systems and bulky alkyl groups participate in a variety of hydrophobic interactions (Fig. 6f, Table 11). These hydrophobic forces in PMRS's core and the surface are much higher in PMRS than EMRS (Fig. 6g, h). Furthermore, the normalized frequency of other electrostatic interactions other than the salt-bridge also dominated in PMRS.

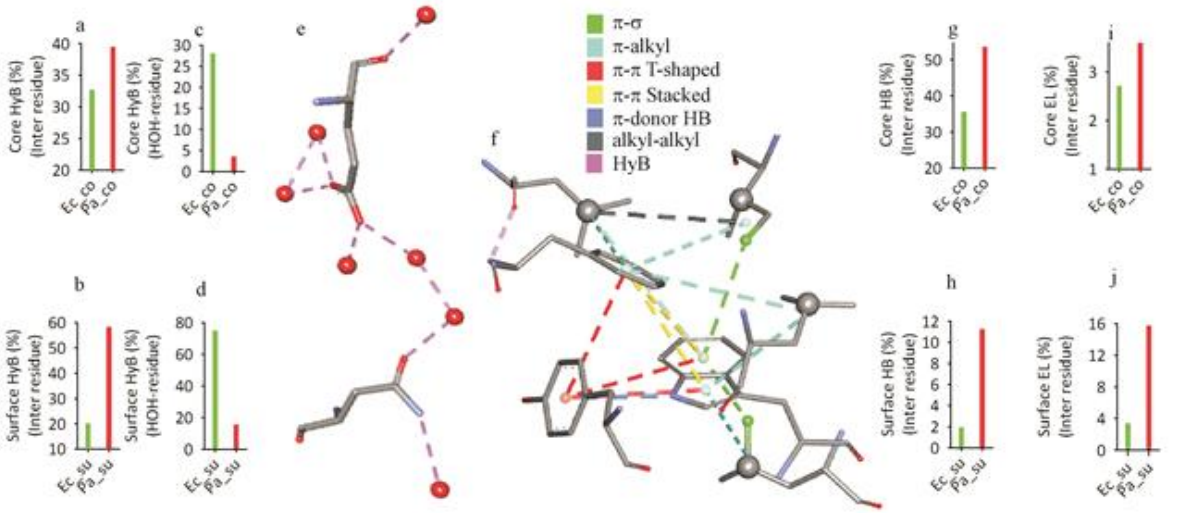

Figure 6: Details on weak interactions other than salt-bridge of PMRS (Pa, red) and EMRS (Ec, green).

Hydrophobic interactions, the most dominant of all weak interactions (Dill, 2005), are more prevalent in PMRS than in EMRS. Just as salt-bridges are important in PMRS's thermostability, so are the higher levels of HyBs and other electrostatic interactions. The latter seems to have some specific roles as their counts are much less (after global normalization) than others. The amount of shell-water in PMRS is much less than in EMRS and so, the HOH-mediated interactions are less. While this may seem counterintuitive in the thermostability of PMRS, the low shell-water, in turn, may enhance collapse-mediated folding and residue packing (Hurley et al., 1992; Russell et al., 1997). Taken together, it can be said that not only the salt-bridge but also other weak interactions are actively involved in PMRS's thermostability.

Cavity at thermostability of PMRS:

The cavity in a folded protein is a highly heterogeneous sub-structure, where, along with the atoms of the protein, shell-waters also participate in its structure. Further, these atoms belong to

the different residue and secondary structure classes. In these aspects, is there any discriminatory feature of the cavity in the thermostability of PMRS compare to EMRS?

Table 11: Normalized frequency of weak forces (except the salt-bridge) in the core and the surface of 1PG2 and 1RQG. Weak forces are divided into hydrogen bond (HyB), hydrophobic and hydrophilic categories. In hydrogen bond there are three sub-categories such as HB/HL, charged and water mediated. In HB/HL, HyB formed by hydrophobic-hydrophobic, hydrophobic-hydrophilic, hydrophilic-hydrophilic residues are included. In charged-mediated HyB, charged-charged, charged-hydrophilic, charged-hydrophobic are included. In water mediated HyB, water-water, water-hydrophobic, water-hydrophilic, water-charged mediated interactions are included. Ion-pair interactions are like salt-bridge where the distance of interaction is greater than 4.0Å. All these interactions were computed using the BIOVIA Discovery Studio 2020 using default parameters for the distance and defined angles. Normalization was done using the total interactions (HyB, hydrophobic, and hydrophilic).

	1PG2_core	1RQG_core	1PG2_surface	1RQG_surface
Hydrogen bond				
HB/HL residue mediated	23.7	28.4	6	8.6
Charged residue mediated	8.9	11	13.9	49.5
Water-mediated	27.9	3.4	74.8	15.3
Hydrophobic				
π-σ	5	8.6	0.2	1.8
π-π	1.9	3.1	0.1	0.8
Amide-π	0.2	0.4	0	0
Alkyl-alkyl	15.8	24.6	0.5	5
π-alkyl	12.5	16.7	1.1	3.6
Hydrophilic				
Ion-pair	0.1	0.8	2.1	12.1
π-cation	0.2	0.2	0.5	0.7
π-anion	0.2	0.1	0.1	0
π-donor HyB	1.4	2.1	0.6	2.5
π-sulfur	0.8	0.4	0	0.4

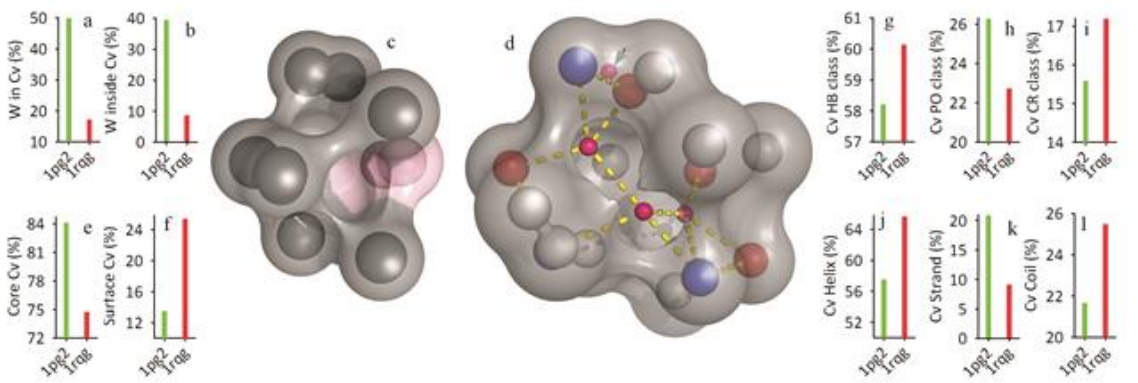

Figure 7: Details on structural components of interior cavities. Here, the red and green bars are of PMRS (1rqg) and EMRS (1pg2), respectively.

(a) Comparison of water (W) containing cavity (Cv). (b) Comparison of inside water-containing cavity. (c) A typical empty cavity. (d) a typical water-filled cavity with water interaction from inside. Arrow indicates an outside W. (e) Comparison of cavity atoms in the core. (f) Comparison of cavity atoms in the surface. (g) Comparison of hydrophobic-class of cavity residues. (h) Comparison of polar-class of cavity residues. (i) Comparison of charged-class of cavity residues. (j) Comparison of cavity atoms in helix. (k) Comparison of cavity atoms in strand. (l) Comparison of cavity atoms in coil.

To check this, we have presented Figure 3. Several points are noteworthy. First, the cavity in PMRS (7.8%) is more than EMRS (5.7%). However, the shell-water-filled total and just inside-filled cavities are almost negligible in PMRS compared to EMRS (Fig. 7a,b) may imply that these types of the cavity are less important in the former (Bandyopadhyay et al., 2019) (Fig. 7c). In EMRA, in inside-filled cavities, the shell-waters form HyBs to themselves and with polar constituents of the cavity to stabilize (Fig. 7d), and thus, make them voluminous. In turn, largely in PMRS, the empty cavity is usually smaller (Vogt et al., 1997), which seems to be stabilized by self-assembly. Second, although the number of cavities in the core is relatively less in PMRS than that of the EMRS, they are highly abundant in its surface regions (Fig. 7e, f). Third, on a residue-class basis, hydrophobic and charged-classes are more in PMRS's cavity than that of EMRS, but polar-class like salt-bridge is less here (Fig. 7g, h, i). Fourth, there are more helix and coil-prone residues in PMRS's cavity than in EMRS.

What is the significance of the above observations in PMRS's thermostability? Since PMRS has more cavities, and since those cavities also show selective preference towards residue-class and secondary structure type, it seems that these cavities are more active in restricting (i.e., packing) these structural elements. Very little shell water inside the cavity of PMRS seems to be another distinct strategy. The abundance of cavities on the PMRS's surface compared to the core demonstrates the importance of surface engineering in thermostability. Taken together, the cavity appears to be an assembler or container of different structural components of protein and, thus, maintains its conformation. In other words, the different elements (especially the secondary structure elements such as helis, strand and coil) would not have come together without these

interior cavities. Since the cavity has a space within itself, it may also have a role in the balance of rigidity and flexibility, which is required in the case of effective proteins in different environments (Dubey and Jagannadham, 2008).

Our study shows that in PMRS, compared to EMRS, salt-bridge and other weak forces and cavities are involved in its thermophilic properties. The importance of the microenvironment is immense as the stability of the salt-bridge towards PMRS is higher than that of EMRS. Regarding PMRS's thermostability in relation to EMRS, its inter-domain and surface engineering are worth noting. These discriminatory structural features seem to stem from its inherent properties in the sequence as about 2/3rd of the homologous position of the former differs from that of the latter. We believe that our study will be applied to other similar systems.

Declaration of competing interest:

There are no competing interests to declare.

Acknowledgments:

We are grateful for the computational facility laboratory of the Department of Biotechnology at the University of Burdwan.

Abbreviations used:

PMRS, Methionine-tRNA synthetase from hyperthermophilic, *Pyrococcus abyssi*; EMRS, Methionine-tRNA synthetase from mesophilic, *E. coli*; ME, microenvironment of salt-bridge; APBS, Adaptive Poisson Boltzmann Solver; SBFR, salt-bridge forming residue; nBSFR, non-salt-bridge forming residue; IP, Isolated pair; NU, Network Unit; IPM, Isolated Pair Method; NUM, Network Unit Method; IPME, isolated pair's partner as ME-candidate; NUME, network unit's partner as ME-candidate; nSBME, ME-candidate but not salt-bridge's partner; HyB, Hydrogen bond

References:

Anfinsen, C. B. (1973). Principles that Govern the Folding of Protein Chains. *Science, 181*(4096), 223–230. https://doi.org/10.1126/science.181.4096.223

Baker, N. A., Sept, D., Joseph, S., Holst, M. J., & McCammon, J. A. (2001). Electrostatics of nanosystems: Application to microtubules and the ribosome. *Proceedings of the National Academy of Sciences, 98*(18), 10037–10041. https://doi.org/10.1073/pnas.181342398

Bandyopadhyay, A. K. (2020). Salt-Bridges in the Microenvironment of Stable Protein Structures. *Bioinformation, 16*(11), 900–909. https://doi.org/10.6026/97320630016900

Bandyopadhyay, A. K., Ul Islam, R. N., Mitra, D., Banerjee, S., & Goswami, A. (2019). Stability of buried and networked salt-bridges (BNSB) in thermophilic proteins. *Bioinformation, 15*(1), 61–67. https://doi.org/10.6026/97320630015061

Bandyopadhyay, A. K., Ul Islam, R. N., Mitra, D., Banerjee, S., & Goswami, A. (2019). Structural insights from water-ferredoxin interaction in mesophilic algae and halophilic archaea. *Bioinformation, 15*(2), 79–89. https://doi.org/10.6026/97320630015079

Banerjee, S., Gupta, P. S. S., Islam, R. N. U., & Bandyopadhyay, A. K. (2021). Intrinsic basis of thermostability of prolyl oligopeptidase from *Pyrococcus furiosus*. *Scientific Reports, 11*(1). https://doi.org/10.1038/s41598-021-90723-4

Banerjee, S., Gupta, P., Nayek, A., Das, S., Sur, V. P., Seth, P., Islam, R. N. U., & Bandyopadhyay, A. K. (2015). PHYSICO2: an UNIX based standalone procedure for computation of physicochemical, window-dependent and substitution based evolutionary properties of protein sequences along with automated block preparation tool, version 2. *Bioinformation, 11*(7), 366–368. https://doi.org/10.6026/97320630011366

Biswas, I., Mitra, D., Bandyopadhyay, A. K., & Das Mohapatra, P. K. (2020). Contributions of protein microenvironment in tannase industrial applicability: An in-silico comparative study of pathogenic and non-pathogenic bacterial tannase. *Heliyon, 6*(11), e05359. https://doi.org/10.1016/j.heliyon.2020.e05359

Crepin, T., Schmitt, E., Blanquet, S., & Mechulam, Y. (2004). Three-Dimensional Structure of Methionyl-tRNA Synthetase from *Pyrococcus abyssi*, *Biochemistry, 43*(9), 2635–2644. https://doi.org/10.1021/bi0356247

Crepin, T., Schmitt, E., Mechulam, Y., Sampson, P. B., Vaughan, M. D., Honek, J. F., & Blanquet, S. (2003). Use of Analogues of Methionine and Methionyl Adenylate to Sample Conformational Changes During Catalysis in Escherichia coli Methionyl-tRNA Synthetase. *Journal of Molecular Biology, 332*(1), 59–72. https://doi.org/10.1016/s0022-2836(03)00917-3

Dill, K. A. (1990). Dominant forces in protein folding. *Biochemistry, 29*(31), 7133–7155. https://doi.org/10.1021/bi00483a001

Dolinsky, T. J., Nielsen, J. E., McCammon, J. A., & Baker, N. A. (2004). PDB2PQR: an automated pipeline for the setup of Poisson-Boltzmann electrostatics calculations. *Nucleic Acids Research, 32*(Web Server), W665–W667. https://doi.org/10.1093/nar/gkh381

Dubey, V., & Jagannadham, M. (2008). Roles for Cavities in Protein Structure: New Insights. *Current Proteomics, 5*(3), 157–160. https://doi.org/10.2174/157016408785909668

Gupta, P., Nayek, A., Banerjee, S., Seth, P., Das, S., Pratap Sur, V., Roy, C., & Bandyopadhyay, A. (2015). SBION2: Analyses of Salt Bridges from Multiple Structure Files, Version 2. *Bioinformation, 11*(1), 39–42. https://doi.org/10.6026/97320630011039

Hurley, J. H., Baase, W. A., & Matthews, B. W. (1992). Design and structural analysis of alternative hydrophobic core packing arrangements in bacteriophage T4 lysozyme. *Journal of Molecular Biology, 224*(4), 1143–1159. https://doi.org/10.1016/0022-2836(92)90475-y

Kumar, S., Ma, B., Tsai, C.J., & Nussinov, R. (2000). Electrostatic strengths of salt bridges in thermophilic and mesophilic glutamate dehydrogenase monomers. *Proteins: Structure, Function, and Genetics, 38*(4), 368–383. https://doi.org/10.1002/(sici)1097-0134(20000301)38:4<368::aid-prot3>3.0.co;2-r

Kumar, S., Tsai, C.J., & Nussinov, R. (2000). Factors enhancing protein thermostability. *Protein Engineering, Design and Selection, 13*(3), 179–191. https://doi.org/10.1093/protein/13.3.179

Martinez, C. R., & Iverson, B. L. (2012). Rethinking the term "pi-stacking. *Chemical Science, 3*(7), 2191. https://doi.org/10.1039/c2sc20045g

Mecozzi, S., West, A. P., & Dougherty, D. A. (1996). Cation-pi interactions in aromatics of biological and medicinal interest: electrostatic potential surfaces as a useful qualitative guide. *Proceedings of the National Academy of Sciences, 93*(20), 10566–10571. https://doi.org/10.1073/pnas.93.20.10566

Menéndez-Arias, L., & Argosf, P. (1989). Engineering protein thermal stability. *Journal of Molecular Biology, 206*(2), 397–406. https://doi.org/10.1016/0022-2836(89)90488-9

Meuzelaar, H., Vreede, J., & Woutersen, S. (2016). Influence of Glu/Arg, Asp/Arg, and Glu/Lys Salt Bridges on α -Helical Stability and Folding Kinetics. *Biophysical Journal, 110*(11), 2328–2341. https://doi.org/10.1016/j.bpj.2016.04.015

Nayek, A., Banerjee, S., & Gupta, P. (2015). ADSETMEAS: Automated Determination of Salt-bridge Energy Terms and Micro Environment from Atomic Structures using APBS method, version 1.0, *Prot. Sci., 24*(2015), 216-217.

Nayek, A., Sen Gupta, P. S., Banerjee, S., Mondal, B., & Bandyopadhyay, A. K. (2014). Salt-Bridge Energetics in Halophilic Proteins. *PLoS ONE, 9*(4), e93862. https://doi.org/10.1371/journal.pone.0093862

Puchkaev, A. V., Koo, L. S., & Ortiz de Montellano, P. R. (2003). Aromatic stacking as a determinant of the thermal stability of CYP119 from *Sulfolobus solfataricus*. Archives of *Biochemistry and Biophysics, 409*(1), 52–58. https://doi.org/10.1016/s0003-9861(02)00402-2

Russell, R. J. M., Ferguson, J. M. C., Hough, D. W., Danson, M. J., & Taylor, G. L. (1997). The Crystal Structure of Citrate Synthase from the Hyperthermophilic Archaeon *Pyrococcus furiosus* at 1.9Å Resolution. *Biochemistry, 36*(33), 9983–9994. https://doi.org/10.1021/bi9705321

Sternke, M., Tripp, K. W., & Barrick, D. (2019). The use of consensus sequence information to engineer stability and activity in proteins. *Methods in Enzymology*, *643*, 149-179. https://doi.org/10.1016/bs.mie.2020.06.001

Sumida, K. H., Núñez-Franco, R., Kalvet, I., Pellock, S. J., Wicky, B. I. M., Milles, L. F., Dauparas, J., Wang, J., Kipnis, Y., Jameson, N., Kang, A., De La Cruz, J., Sankaran, B., Bera, A. K., Jiménez-Osés, G., & Baker, D. (2024). Improving Protein Expression, Stability, and Function with ProteinMPNN. *Journal of the American Chemical Society, 146*(3), 2054–2061. https://doi.org/10.1021/jacs.3c10941

Szilágyi, A., & Závodszky, P. (2000). Structural differences between mesophilic, moderately thermophilic and extremely thermophilic protein subunits: Results of a comprehensive survey. *Structure*, *8*(5), 493-504. https://doi.org/10.1016/S0969-2126(00)00133-7

Tsodikov, O. V., Record, M. T., & Sergeev, Y. V. (2002). Novel computer program for fast exact calculation of accessible and molecular surface areas and average surface curvature. *Journal of Computational Chemistry, 23*(6), 600–609. Portico. https://doi.org/10.1002/jcc.10061

Vogt, G., Woell, S., & Argos, P. (1997). Protein thermal stability, hydrogen bonds, and ion pairs. *Journal of Molecular Biology*, *269*(4), 631–643. https://doi.org/10.1006/jmbi.1997.1042

Williams, R. W., Chang, A., Juretić, D., & Loughran, S. (1987). Secondary structure predictions and medium range interactions. *Biochimica et Biophysica Acta (BBA) - Protein Structure and Molecular Enzymology*, *916*(2), 200–204. https://doi.org/10.1016/0167-4838(87)90109-9

Yip, K. S. P., Britton, K. L., Stillman, T. J., Lebbink, J., de Vos, W. M., Robb, F. T., Vetriani, C., Maeder, D., & Rice, D. W. (1998). Insights into the molecular basis of thermal stability from the analysis of ion-pair networks in the Glutamate Dehydrogenase family. *European Journal of Biochemistry*, *255*(2), 336–346. Portico. https://doi.org/10.1046/j.1432-1327.1998.2550336.x

HOW TO CITE

Sahini Banerjee and Amal Kumar Bandyopadhyay (2024). *Pyrococcus abyssi*'s Methionine-tRNA Synthetase Exhibits Hyperthermophilic Signatures in its Weak Forces and Cavities. © International Academic Publishing House (IAPH), Dr. Somnath Das, Dr. Jayanta Kumar Das, Dr. Mayur Doke and Dr. Vincent Avecilla (eds.), *Life as Basic Science: An Overview and Prospects for the Future Volume: 3*, pp. 180-208. ISBN: 978-81-978955-7-9. doi: https://doi.org/10.52756/lbsopf.2024.e03.008